DYNAMIC CHARACTERISTICS OF AN OVERHUNG P/A FAN IN ROLLING ELEMENT AND FLUID FILM BEARINGS

By

E. J. Gunter, *Professor*

Department of Mechanical and Aerospace Engineering

University of Virginia, Charlottesville, Va.

Alex Hobbs, *Principal Research Engineer*

Carolina Power and Light, Raleigh, North Carolina

C. Phelps, *Senior Engineer*

Carolina Power and Light, Raleigh, North Carolina

ABSTRACT

This paper concerns the experimental and theoretical investigation of a class of overhung primary air utility fans mounted in rolling element and fluid film bearings. This particular class of fan has led to considerable difficulties in balancing and bearing life. An experimental investigation of the fans mounted in rolling element bearings indicated that the fans are operating at the 1st critical speed.

The overhung rotor in rolling element bearings was extremely difficult to balance because of its operation in the vicinity of a critical speed, higher order harmonics and lack of damping in the rotor-bearing system.

A detailed theoretical analysis of the fan critical speed in rolling element bearings indicated that the critical speed should have been 15 to 20 % above the operating speed range. The reduction in fan critical speed to below the operating speed range was caused in part by the flexibility of the overhung disk, and also by flexibility or elasticity of the fan end bearing support structure.

One of the fans was replaced with fluid film bearings. It is shown that the fluid film bearings have effectively higher stiffness and damping than the rolling element configuration. A satisfactory balance was possible with the fan in fluid film bearings, whereas in the case of the rolling element bearings, accurate balancing could not be achieved. The bearing forces transmitted with fluid film bearings may be reduced in half by reducing the shaft diameter of the overhang section.

An elastomeric isolation support was designed for the fan end rolling element bearing to reduce the critical speed to below the operating speed range. It is demonstrated that the isolation support reduces the forces transmitted to the fan rolling element bearing by a factor of 20 at running speed. Extended bearing life and ease of field balancing was achieved by using the isolation support system with the rolling element bearings.

1 INTRODUCTION AND BACKGROUND

This paper presents some of the vibration characteristics and the analysis performed on a number of utility overhang primary air fans. This class of fan has been a continuous operational problem for the utility. There are four of these fans in service at the utility fossil facility. High rotor and pedestal vibrations have caused numerous bearing failures and the fans have been difficult to balance. The fan assembly weighs approximately 1,500 lb. and operates at 1,800 RPM. It is used to supply primary air to the boilers.

The original fans were designed with fluid film journal bearings. High fan end pedestal vibrations were encountered with the original fluid film bearings. These high vibrations caused some ruptures in the cooling water lines to the bearing caps. The original fluid film sleeve bearings were then replaced with anti-friction rolling element bearings.

Figure 1 represents a schematic outline of a typical primary air (P/A) fan installation with fluid film bearings mounted on a concrete foundation. Figure 2 represents a schematic of the modified P/A fans mounted on rolling element bearings. Four P/A fans were modified with various bearing spans and overhang distances as shown in Figure 2. The original P/A fan bearing spans were 22 inches with an overhang distance of approximately 22 inches. The fan wheel weight of 1,000 lb cause a fan bearing static loading of 2,000 lb, but an uploading of 1,000 lb on the motor end bearing.

After replacement of the fluid film bearings with rolling element bearings in the B-Fan, it was found that the fan was very sensitive to minor unbalance. This high sensitivity to unbalance was due to the low level of damping in the system caused by the use of rolling element bearings, and also due to the condition that the fan was operating near a critical speed.

At the time the fluid film bearings were replaced by rolling element bearings, it was thought that the fans were operating in the subcritical speed region. It is standard practice with this class of fan to design the critical speed to be 20 % above the operating speed range. Later tests on the B fan showed that, with the rolling element bearings, the B fan was operating slightly above the first critical speed rather than 20 % below it.

A study of the fan vibration problem was initiated by the utility research center in 1983 in order to determine the nature of the vibration and to propose a design remedy. Preliminary critical speed based calculations were performed based on the transfer matrix method of Colen. In the original critical speed analysis, assuming a bearing stiffness value of 2E6 lb/in., a first critical speed of 3,577 RPM was computed assuming that the fan wheel was rigid. However, this design of fan impeller has been known to be very flexible. A flexible disc cannot transmit the theoretical rigid disc gyroscopic moment to the shaft, and hence the actual critical speed will not be as high as that predicted for the case of an ideal rigid fan disc *(Kikuchi)*.

The rigid fan polar and transverse moments of inertia, Ip and It were computed to be 583,685 $lb - in^2$ and 330, 733 $lb - in^2$ respectively, with a corresponding fan weight of 1,010 lb. To simulate a flexible fan in the earlier analysis, the disc polar moment of inertia Ip was reduced by a factor of 10 from 583,685 $lb - in^2$ to 58,368 $lb - in^2$. This reduction in the polar moment of inertia, to simulate a flexible disc, caused a reduction in the first critical speed from 3,577 RPM to less than half that value, 1,723 RPM. This particular calculation showed dramatically the importance of disc flexibility in reducing the critical speed of an overhung rotor.

A more advanced transfer matrix critical speed program was developed to handle the special

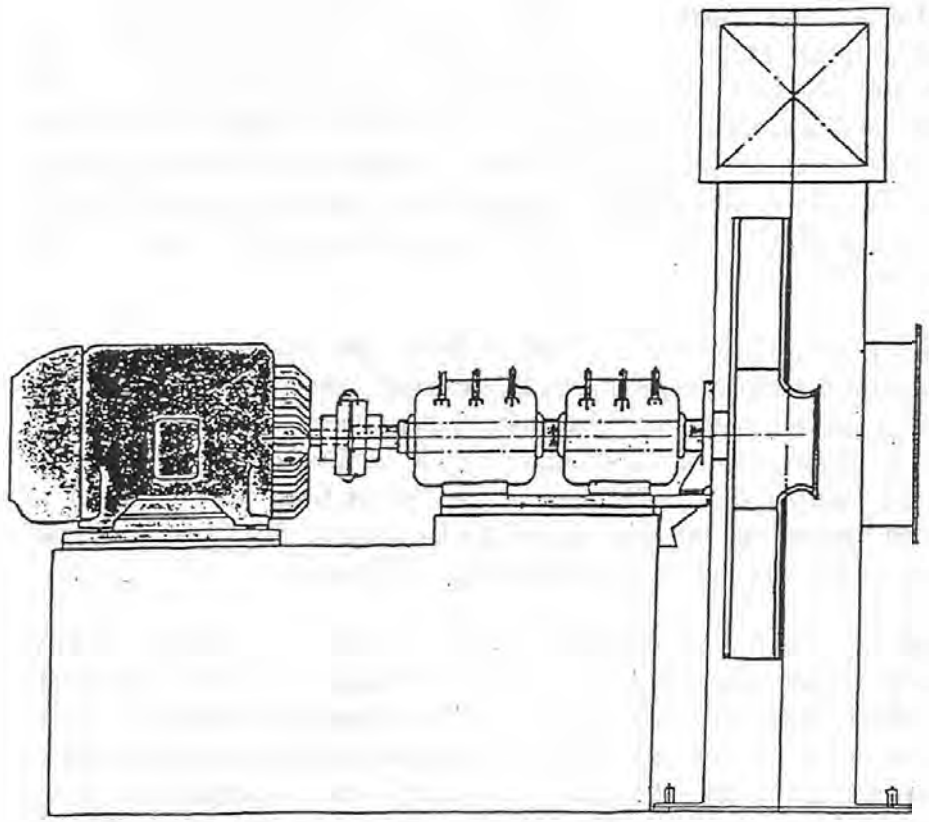

FIGURE 1. SCHEMATIC OF OVERHUNG P/A FAN IN ORIGINAL FLUID FILM BEARINGS

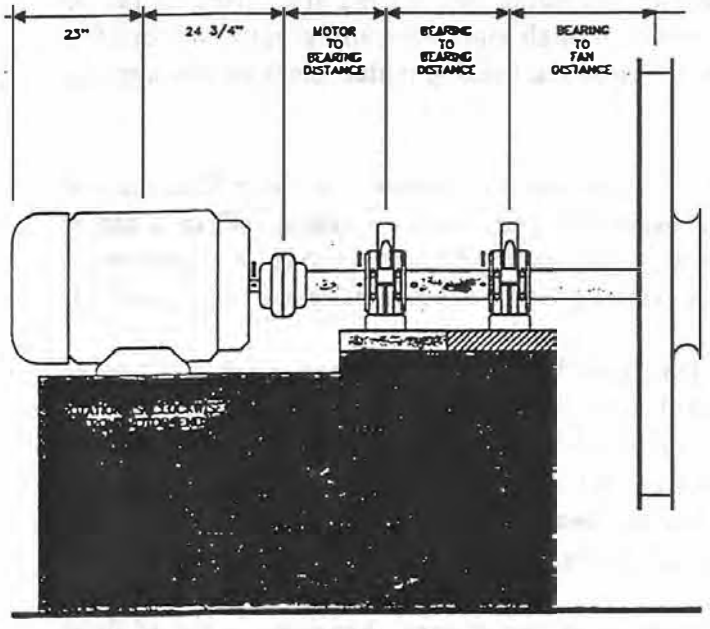

FAN	A	B	C	D
MOTOR TO BEARING	NA	15 1/2"	15 1/2"	17"
BEARING TO BEARING	NA	22"	27 1/4"	26 1/4"
BEARING TO FAN	NA	22"	16 1/4"	16 1/4"

Key
- X AXIS PROXIMETER PROBE
- Y AXIS PROXIMETER PROBE
- X AXIS KEY PHASOR

FIGURE 2. SCHEMATIC OF MODIFIED OVERHUNG P/A FANS WITH ROLLING ELEMENT BEARINGS

case of flexibly mounted offset discs *(Gaston and Gunter)*. In addition to the fan flexibility effect, pedestal mass and support stiffness play an important role in reducing the overall bearing impedance *(Barrett)*, *(Kirk)*. Flexible pedestals were also incorporated into the program. Extreme care must be taken when incorporating branched systems into an undamped transfer matrix critical speed analysis due to the occurrence of numerical instability caused by singular branch roots. The theory of undamped critical speeds of multi-speed turborotors with flexible discs and pedestal effects and the removal of singular branch roots was presented by Kazao and Gunter in 1987.

At the time of the preliminary critical speed analysis in 1983, there was no experimental data available to ascertain the fan critical speed in rolling element bearings. Vibration data was later obtained on the B fan for startup and shutdown. Figure 3 represents the vibration data taken on the B fan in 1983 with an IRD 360 analyzer with the filter out. The vibration measurement was recorded with an IRD shaft rider at a 45° angle from the vertical at a measurement plane located between the fan bearing and the fan air seal. Note that a critical speed of 1,720 RPM is recorded on startup with an amplitude of 22 mils.

The amplitude diminishes rapidly after the fan passes through its first critical speed. The rapid drop off in amplitude is very characteristic of nonlinear bearing behavior under high rotating loads. On shut down, under no motor drive torque conditions, the critical speed is reduced to 1,520 RPM due to the removal of the drive torque from the system, and loading effects caused by a misaligned motor-fan. An unloaded rolling element bearing with dead band (bearing radial clearance), for example, will appear to have a lower critical speed than will a loaded rolling element bearing. At the time these vibration measurements were made, no phase angle measurements were recorded.

Because of the balancing difficulties encountered with the replacement rolling element bearings, it was decided to reduce the fan overhang in order to elevate the rotor 1*st* critical speed. This was accomplished in several of the fans by increasing the bearing span from 22 in. to over 26 in. These fans also had the characteristics of high vibrations and greatly reduced fan bearing life. The C and D fans, for example, required fan bearing replacement on the average of every 6 months.

The logic assumed for increasing the bearing span was to increase the rotor first critical speed, so that the fans would be operating below their first critical speed. When a fan is operating below its 1*st* critical speed, however, high bearing forces may still be encountered at the fan bearing even though the rotor is operating in the subcritical speed region *(Kirk)*.

The reason for this is because the Dynamic Transmissibility Ratio parameter, TRD, is always greater than one. This parameter is the ratio of the transmitted bearing forces to the rotating unbalance forces. With this fan, the TRD may be 20-50 or greater under certain conditions. This implies that the fan bearing force transmitted may be 50 times or more larger than the rotating unbalance load. With rolling element bearings, the bearing L_{10} life is inversely proportional to the cube of the bearing loading. Hence, short bearing life may be anticipated.

Because of the difficulty in balancing the fans in rolling element bearings, a set of fluid film bearings were reinstalled in the A-Fan with the original bearing span of 22 in. Experimental tests indicate that the fluid film bearings actually provide a higher effective stiffness than the rolling element bearings. The A fan is operating below the 1*st* critical speed with fluid film bearings as shown in Figure 4. However, because of the excellent damping of the fluid film bearings, the rotor may be balanced with greater ease than the other fans supported in rolling element bearings.

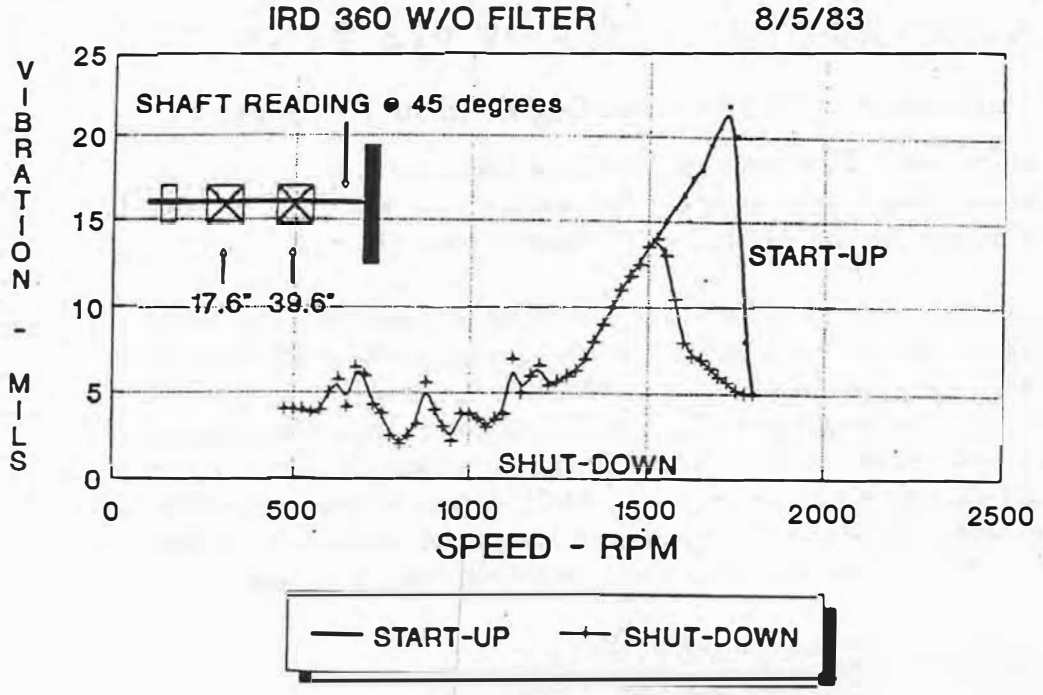

FIGURE 3. **TOTAL VIBRATION OF B FAN WITH IRD 360 ANALYZER FOR RUN-UP AND RUN-DOWN WITH THE FILTER OUT**

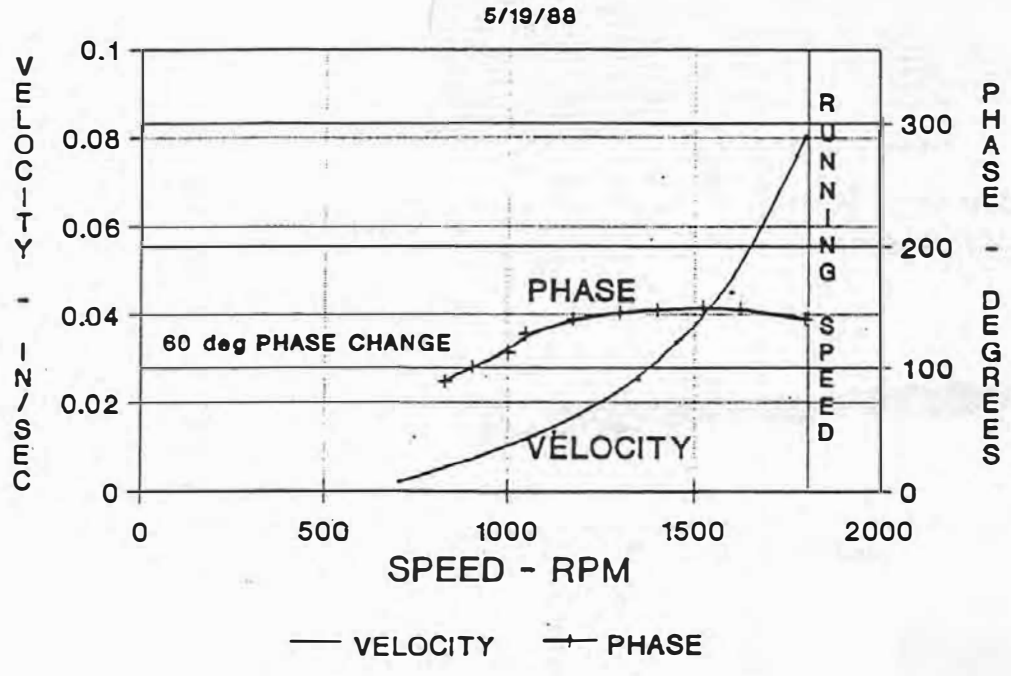

FIGURE 4. **HORIZONTAL A FAN FLUID FILM BEARING HOUSING SYNCHRONOUS VELOCITY AND PHASE DURING RUNUP (IN/SEC)**

2 VIBRATION CHARACTERISTICS OF P/A FANS

2.1 Vibration Characteristics of B Fan in Rolling Element Bearings.

The fans were instrumented with shaft displacement probes at the motor and fan end bearings and velocity pickups at the bearing pedestals. The vibration data was collected using both the CSI Wave Pack System and the Bently Nevada Digital Vector Filter II.

Figure 5 represents a waterfall or cascade diagram of the B fan vertical displacement at the No. 2 or fan bearing location obtained during a coast down run with rolling element bearings. Figure 6 represents the total motion vs. time. The wave form maximum amplitude was set at 12 mils which caused the clipping of the signal. It is apparent that the amplitude increases when the B fan is shut down. This is caused by the fan passing through the first critical speed. A frequency analysis of the spectrum at 1,728 RPM shows a synchronous and a second harmonic component of over twice the synchronous component. After the fluid film bearings were placed in the B unit, the second harmonic component was not present.

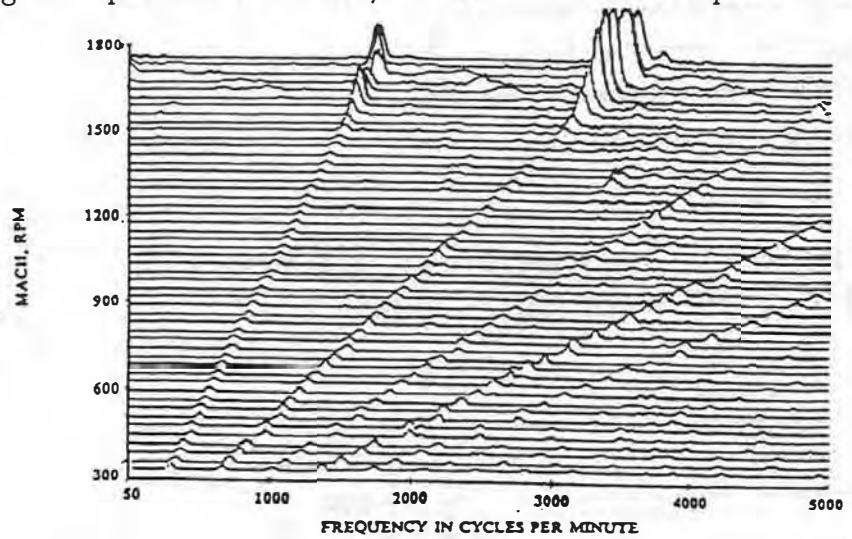

FIGURE 5. FREQUENCY SPECTRUM PLOT OF B FAN VERTICAL BEARING MOTION DURING COAST DOWN

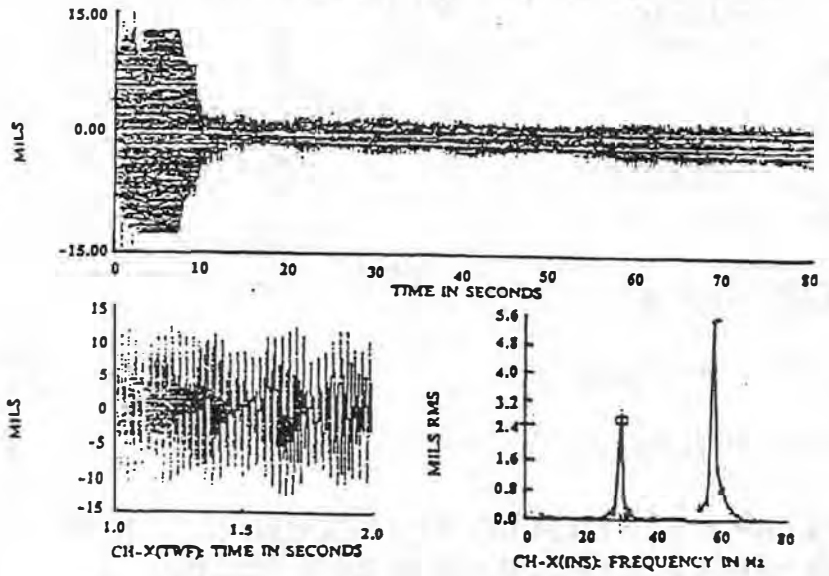

FIGURE 6. TIME TRANSIENT HISTORY OF B FAN VERTICAL BEARING MOTION DURING COAST DOWN

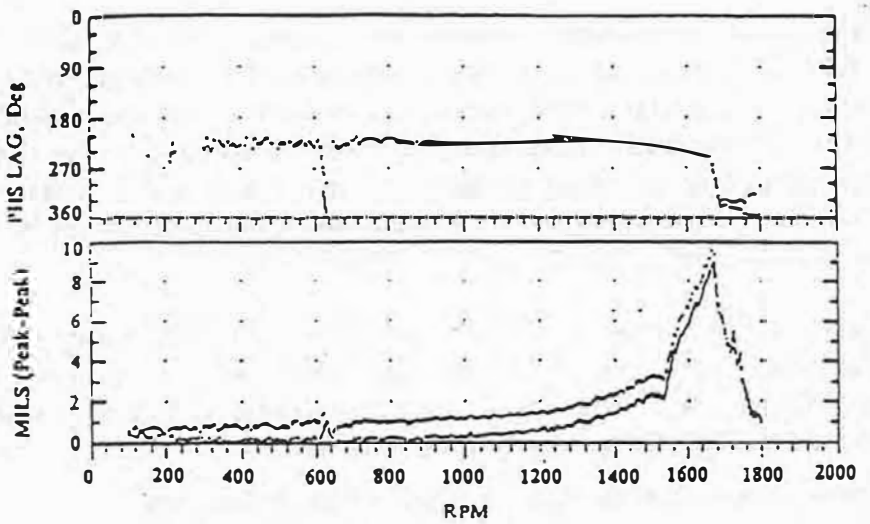

FIGURE 7. B FAN HORIZONTAL FAN BEARING SYNCHRONOUS AMPLITUDE AND PHASE DURING COAST DOWN (MILS P-P)

Figure 7 represents the fan bearing horizontal pedestal synchronous motion observed during shutdown. Note that a distinct critical speed around 1,680 RPM was observed with a synchronous amplitude of almost 10 mils! This high amplitude could easily cause a dynamic bearing loading of over 4,000 lb. on the fan end bearing. Balancing of the B fan is extremely difficult since it is operating in the vicinity of a critical speed and also since it has a 2nd harmonic component which is larger than the synchronous component.

2.2 Vibration Characteristics of A Fan in Rolling Element Bearings.

Figure 8 represents the synchronous vertical motion of the A fan bearing. This fan had the bearing span increased from 22 in. to 26.75 in. This change in bearing span reduced the amount of the fan wheel overhang and hence raised the critical speed. In this case, it can be seen from Figure 8 that the critical speed is above the operating speed range.

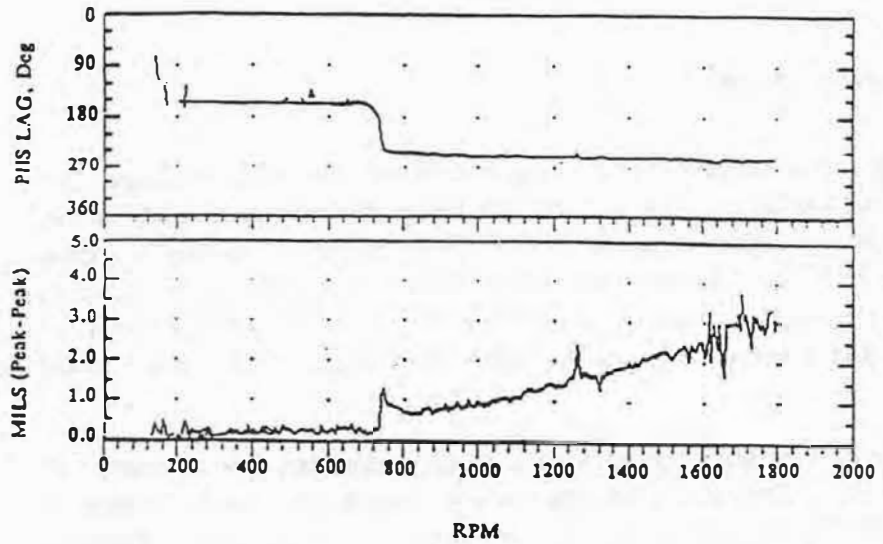

FIGURE 8. VERTICAL A FAN SYNCHRONOUS AMPLITUDE AND PHASE DURING COAST DOWN (MILS P-P)-26 IN BEARING SPAN

The amplitude of motion caused by unbalance increases with speed. At 1,800 RPM, the amplitude was almost 4.0 mils. whereas the B fan motion had reduced to approximately 1.5 mils since it was operating above its 1*st* critical speed. The A fan end bearing dynamical forces caused by unbalance will be much higher than the forces transmitted to the B end bearing fan for the same amount of fan wheel unbalance. The reason for this is that the B fan is operating in the supercritical speed region, whereas the A fan is operating in the subcritical speed region with a higher bearing dynamic transmissibility.

Of interest also in Figure 8 is the observed jump in amplitude at 720 RPM along with a corresponding phase shift. This indicates a possible foundation mode which may have been induced by the failure of the grouting under the A fan bearing pedestal due to the high dynamical loads transmitted through the fan end bearing pedestal.

2.3 Vibration Characteristics of A Fan in Fluid Film Bearings.

The rolling element bearings were removed from the A fan and replaced by fluid film bearings. The bearing span was returned to the original condition of 22 in. The A fan therefore was similar to the B fan except that the A fan was now installed with fluid film bearings whereas the B fan was configured with rolling element bearings. Fan bearing cap velocity measurements were recorded during startup.

The pedestal motion gradually increased to 0.076 in/sec with a corresponding phase increase of 60° as shown in Figure 4. There was no indication of large sub or supersynchronous vibrations. The motion of the A fan was well behaved. The phase change of only 60° is an indication that the fan is operating in the subcritical speed vicinity. No problem was encountered with balancing the A fan in fluid film bearings. A failure of the fan end bearing was encountered during startup after shutdown from several months of operation and a gradual buildup of unbalance due to dust accumulation on the blades. Since the fan is operating in the subcritical speed region, it is still sensitive to fan wheel unbalance. The bearing failure encountered during startup was attributed to the lack of a forced lubrication system and excessive babbet thickness.

3 Critical Speed Analysis of P/A Fans

3.1 Description of Rotor Model.

The P/A fans are overhung rotors supported by rolling element or fluid film bearings. The shaft diameter at the bearing locations is 5.0 in. and the design bearing span is 22 inches. The overhang distance to the fan center of gravity is 22 inches. Figure 9 represents a cross sectional outline of a typical P/A fan. The fan is supported by 2 bearing housings mounted on a concrete pedestal. Figure 9 shows the fan original bearing span of 22 in. and the extended bearing span used on the C and D fans. From this schematic diagram, a critical speed model was developed.

The P/A fans were modeled as 17 station rotors with a flexibly mounted disc at station 16 (*Gaston and Gunter*). The characteristics of the fan weight, length and inertia properties are shown in Table 1. The flexible disc at station 16 is assumed to have its center of gravity offset from the point of attachment to the shaft by 3.75 in. The disc is assumed attached to the shaft by means of a rotational spring K_r (in-lb/rad). This rotational spring is used to represent the flexibility of the disc. The assumption of a flexible offset disc, instead of a rigidly attached disc, has a significant influence on the critical speed.

TABLE 1. FAN MODEL FOR CRITICAL SPEED ANALYSIS

P/A B FAN WITH ROLLING ELEMENT BEARINGS-Wf-280 Lb,Kf-1.5E6 Lb/IN.
BEARING STIFFNESS - 1.5E6 Lb/In., DISC ROTATIONAL Kr-1.35E7-Lb-IN./rad
BEARING SPAN - 22 IN. , Wfan-1,010 Lb ,Ip-583,685, It-330,733 Lb-In^2

Number of MASS STATIONS - 17
Number of BEARINGS - 2
Number of ATTACHED DISCS - 0
Number of OFFSET FLEXIBLE DISCS - 1
Number of MODES TO CALCULATE - 2
Default Density - 2.83E-01 Lb/In^3
Default Young's Modulus - 3.00E+07 Lb/In^2

Distributive Shaft Gyroscopics ARE NOT INCLUDED in Model.
Transverse Shear Deformation IS NOT INCLUDED in Shaft Calculations.
Input data are in ENGLISH units.
Output data are in ENGLISH units.

---- FLEXIBLE OFFSET DISC DATA ----

ST #	DISC WEIGHT Lb	ROT STIFF Lb-In/Rad	EXT DIA In	INT DIA In	DISC THICK In	DISC DENS Lb/In^3	DISC OFFSET In	POLAR MOMENT Lb-In^2	TRANS MOMENT Lb-In^2
16	1010.00	1.35E+07	33.00	4.00	7.50	1.00E-07	3.75	5.83E+05	3.30E+05

Natural Frequency of Disc # 1 - 999999.0 RPM

-- COMPLETE ROTOR MODEL --

ST #	ST LENGTH In	ST WEIGHT Lb	EXT DIA In	INT DIA In	ST DENSITY Lb-In^3	EI Lb-In^2	POLAR MOMENT Lb-In^2	TRANS MOMENT Lb-In^2	Z Pos In
1	1.50	22.24	11.55	0.00	2.83E-01	2.62E+10			0.0
2	2.00	34.74	7.50	0.00	2.83E-01	4.66E+09			1.5
3	4.25	20.06	4.00	0.00	2.83E-01	3.77E+08			3.5
4	3.88	18.32	5.00	0.00	2.83E-01	9.20E+08			7.8
5	3.88	21.53	5.00	0.00	2.83E-01	9.20E+08			11.6
6	4.40	22.99	5.00	0.00	2.83E-01	9.20E+08			15.5
7	4.40	24.45	5.00	0.00	2.83E-01	9.20E+08			19.9
8	4.40	24.45	5.00	0.00	2.83E-01	9.20E+08			24.3
9	4.40	24.45	5.00	0.00	2.83E-01	9.20E+08			28.7
10	4.40	24.45	5.00	0.00	2.83E-01	9.20E+08			33.1
11	4.38	24.38	5.00	0.00	2.83E-01	9.20E+08			37.5
12	4.38	24.31	5.00	0.00	2.83E-01	9.20E+08			41.9
13	4.38	24.31	5.00	0.00	2.83E-01	9.20E+08			46.3
14	4.38	24.31	5.00	0.00	2.83E-01	9.20E+08			50.6
15	2.50	17.29	4.30	0.00	2.83E-01	5.03E+08			55.0
16	4.00	12.25	4.00	0.00	2.83E-01	3.77E+08			57.5
17	0.00	7.11	4.00	0.00	2.83E-01	3.77E+08			61.5

TOTALS: Length - 61.50 In Trans Moment (about cg) - 7.90E+05 Lb-In^2
Weight - 1381.65 Lb Polar Moment - 5.83E+05 Lb-In^2

Center of Gravity is 51.90 In from left end

Average Diameter - 5.31 In Average Length - 3.84 In
Average Weight - 86.35 Lb Average EI - 2.51E+09 Lb-In^2

L1avg - 4.92E-09 L2avg - 1.01E-08 L3avg - 1.42E-08 (Internal Scale Factors)

-- BEARING and FLEXIBLE PEDESTAL DATA --

BRG LOC (ST #)	BEARING STIFFNESS (Lb/In)	SUPPORT STIFFNESS (Lb/In)	SUPPORT WEIGHT (Lb)	-- RESONANT FREQUENCIES -- SUPPORT ONLY (RPM)	SUPPORT/BRG (RPM)
6	1500000	1500000	280.00	13732	19420
11	1500000	1500000	280.00	13732	19420

TABLE 1. FAN MODEL FOR CRITICAL SPEED ANALYSIS

P/A B FAN WITH ROLLING ELEMENT BEARINGS-Wf=280 Lb,Kf=1.5E6 Lb/IN.
BEARING STIFFNESS = 1.5E6 Lb/In., DISC ROTATIONAL Kr=1.35E7 Lb-IN./rad
BEARING SPAN = 22 IN. , Wfan=1,010 Lb ,Ip=583,685, It=330,733 Lb-In^2

Number of MASS STATIONS = 17
Number of BEARINGS = 2
Number of ATTACHED DISCS = 0
Number of OFFSET FLEXIBLE DISCS = 1
Number of MODES TO CALCULATE = 2
Default Density = 2.83E-01 Lb/In^3
Default Young's Modulus = 3.00E+07 Lb/In^2

Distributive Shaft Gyroscopics ARE NOT INCLUDED in Model.
Transverse Shear Deformation IS NOT INCLUDED in Shaft Calculations.
Input data are in ENGLISH units.
Output data are in ENGLISH units.

---- FLEXIBLE OFFSET DISC DATA ----

ST #	DISC WEIGHT Lb	ROT STIFF Lb-In/Rad	EXT DIA In	INT DIA In	DISC THICK In	DISC DENS Lb/In^3	DISC OFFSET In	POLAR MOMENT Lb-In^2	TRANS MOMENT Lb-In^2
16	1010.00	1.35E+07	33.00	4.00	7.50	1.00E-07	3.75	5.83E+05	3.30E+05

Natural Frequency of Disc # 1 = 999999.0 RPM

-- COMPLETE ROTOR MODEL --

ST #	ST LENGTH In	ST WEIGHT Lb	EXT DIA In	INT DIA In	ST DENSITY Lb-In^3	EI Lb-In^2	POLAR MOMENT Lb-In^2	TRANS MOMENT Lb-In^2	Z Pos In
1	1.50	22.24	11.55	0.00	2.83E-01	2.62E+10			0.0
2	2.00	34.74	7.50	0.00	2.83E-01	4.66E+09			1.5
3	4.25	20.06	4.00	0.00	2.83E-01	3.77E+08			3.5
4	3.88	18.32	5.00	0.00	2.83E-01	9.20E+08			7.8
5	3.88	21.53	5.00	0.00	2.83E-01	9.20E+08			11.6
6	4.40	22.99	5.00	0.00	2.83E-01	9.20E+08			15.5
7	4.40	24.45	5.00	0.00	2.83E-01	9.20E+08			19.9
8	4.40	24.45	5.00	0.00	2.83E-01	9.20E+08			24.3
9	4.40	24.45	5.00	0.00	2.83E-01	9.20E+08			28.7
10	4.40	24.45	5.00	0.00	2.83E-01	9.20E+08			33.1
11	4.38	24.38	5.00	0.00	2.83E-01	9.20E+08			37.5
12	4.38	24.31	5.00	0.00	2.83E-01	9.20E+08			41.9
13	4.38	24.31	5.00	0.00	2.83E-01	9.20E+08			46.3
14	4.38	24.31	5.00	0.00	2.83E-01	9.20E+08			50.6
15	2.50	17.29	4.30	0.00	2.83E-01	5.03E+08			55.0
16	4.00	12.25	4.00	0.00	2.83E-01	3.77E+08			57.5
17	0.00	7.11	4.00	0.00	2.83E-01	3.77E+08			61.5

TOTALS: Length = 61.50 In Trans Moment (about cg) = 7.90E+05 Lb-In^2
Weight = 1381.65 Lb Polar Moment = 5.83E+05 Lb-In^2

Center of Gravity is 51.90 In from left end

Average Diameter = 5.31 In Average Length = 3.84 In
Average Weight = 86.35 Lb Average EI = 2.51E+09 Lb-In^2

L1avg = 4.92E-09 L2avg = 1.01E-08 L3avg = 1.42E-08 (Internal Scale Factors)

-- BEARING and FLEXIBLE PEDESTAL DATA --

BRG LOC (ST #)	BEARING STIFFNESS (Lb/In)	SUPPORT STIFFNESS (Lb/In)	SUPPORT WEIGHT (Lb)	-- RESONANT FREQUENCIES -- SUPPORT ONLY (RPM)	SUPPORT/BRG (RPM)
6	1500000	1500000	280.00	13732	19420
11	1500000	1500000	280.00	13732	19420

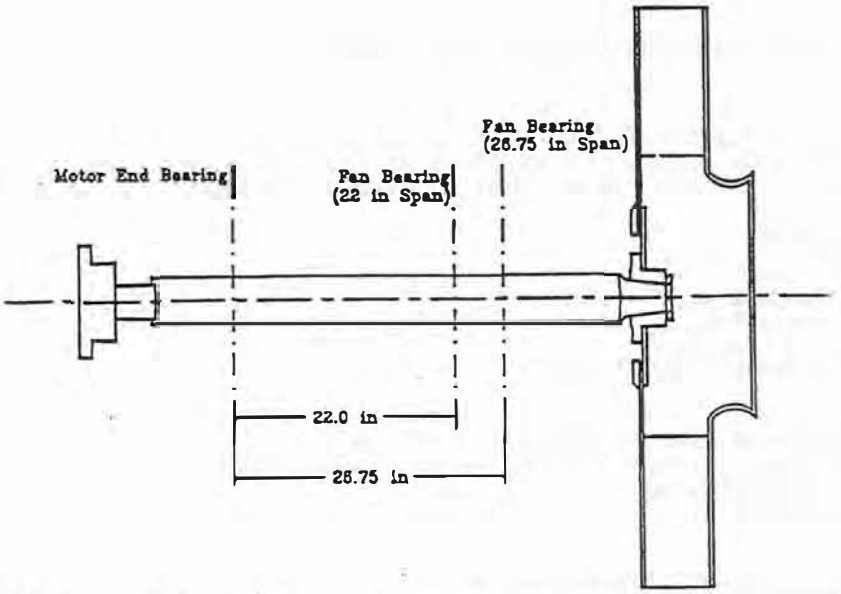

FIGURE 9. SCHEMATIC OUTLINE OF P/A FAN ROTOR SHOWING STANDARD AND MODIFIED BEARING SPANS

In this model, a rotational stiffness of $K_r = 1.35E7$ in-lb was chosen based on a finite element analysis of the fan wheel. An effective rotational spring rate may also be determined from a rap test of the fan disc to determine its natural ringing frequency. The disc 1^{st} diametral ringing frequency is proportional to the square root of the ratio of the rotational stiffness K_r divided by the disc transverse moment of inertia I_t.

3.2 Critical Speed Analysis.

A number of critical speed calculations were performed on the fans assuming various combinations of bearing span, bearing/pedestal stiffnesses, and disc rotational stiffness values K_r. The combination of these factors leads to a wide range of possibilities for the occurrence of the fan first critical speed. By comparing the predicted 1^{st} critical speed with the experimental B fan rotor behavior, it was possible to develop a realistic rotor model that was used for the later calculations of rotor unbalance response.

3.2.1 Influence of Disc Flexibility and Offset Distance.

In the initial critical speed computations, a first critical speed as high as 3,577 RPM was predicted assuming a bearing stiffness of 2.0E6 lb/in. This high value of critical speed was obtained assuming that the fan disc was perfectly rigid, and that the point of disc attachment to the shaft was at the disc center of gravity.

Upon close examination of the fan design, and based upon experiences with other large built up fans, it was felt that the fan wheel is not perfectly rigid, but is in fact flexible. A finite element model of the fan was developed and the first 6 fan modes were computed using the MSC PAL2 finite element program.

The assumption of a flexible disc causes a reduction of the gyroscopic moments transmitted

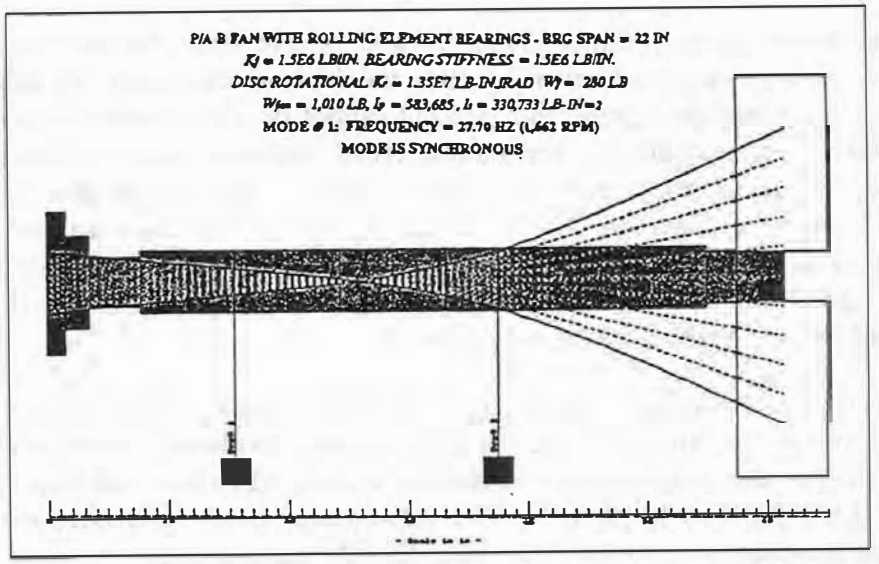

FIGURE 10. ANIMATED 1ST CRITICAL SPEED MODE SHAPE

TABLE 2. 1ST CRITICAL SPEED MODE SHAPE - 1,662 RPM

P/A B FAN WITH ROLLING ELEMENT BEARINGS-Wf=280 Lb,Kf=1.5E6 Lb/IN.
BEARING STIFFNESS = 1.5E6 Lb/In., DISC ROTATIONAL Kr=1.35E7 Lb-IN./rad
BEARING SPAN = 22 IN. , Wfan=1,010 Lb ,Ip=583,685, It=330,733 Lb-In^2

UNDAMPED ROTOR MODESHAPE & ENERGY DISTRIBUTION
SYNCHRONOUS CRITICAL SPEED ANALYSIS

FIRST CRITICAL SPEED = 1661.89 RPM (27.70 HZ) Delta = 6.50e-08

ST. #	X DIM	THETA SLOPE	M MOMENT	V SHEAR	Ushaft STRAIN ENERGY %	Ubrg ENERGY %	KeTran KINETIC ENERGY %	KeRot ENERGY %
1	-0.205	0.01	0.0	0.0			0.1	0.0
2	-0.193	0.01	-0.5	-0.4			0.2	0.0
3	-0.178	0.01	-2.3	-0.9			0.1	0.0
4	-0.146	0.01	-7.3	-1.2			0.0	0.0
5	-0.117	0.01	-12.6	-1.4			0.0	0.0
6	-0.088	0.01	-18.7	-1.6	0.2	4.5	0.0	0.0
7	-0.055	0.01	262.0	63.8	1.3		0.0	0.0
8	-0.016	0.01	542.3	63.7	3.6		0.0	0.0
9	0.035	0.01	822.4	63.7	7.0		0.0	0.0
10	0.102	0.02	1102.8	63.7	11.7		0.0	0.0
11	0.193	0.02	1384.1	63.9	11.0	21.7	0.1	0.0
12	0.310	0.03	1036.0	-79.6	5.7		0.3	0.0
13	0.449	0.03	690.4	-79.0	2.1		0.6	0.0
14	0.602	0.04	348.7	-78.1			1.1	0.0
15	0.762	0.04	11.9	-77.0			1.2	0.0
**	0.941	0.023			3.8		110.6	-16.8
16	0.854	0.04	-177.9	-75.9			1.1	0.0
17	1.000	0.04	0.0	-0.6			0.9	0.0
Total Rotor Energy					42.91%	26.26%	5.83%	0.00%
** Flexible Disk Energy					3.79%		110.56%	-16.78%

Brg #	St. #	K Brg Lb/In	K Eff Lb/In	Xbrg DIM	Xsup DIM	Ubrg %	Usup %	KE Sup %
1	6	1500000	744467	-0.09	-0.04	4.51	4.65	0.07
2	11	1500000	744467	0.19	0.10	21.75	22.40	0.33

U Total = 3.17e+04 KE Total = 3.17e+04 Energy Balance = 0.00 % Error

to the shaft. When the fan polar moment of inertia I_p is greater than the fan transverse moment of inertia I_t , the gyroscopic moment elevates the first critical speed. If, however, the fan disc flexes, then the complete gyroscopic moment cannot be transmitted to the shaft. This causes a reduction in the predicted rotor critical speed. Another factor which causes a reduction in the gyroscopic moment transferred is the fan axial offset distance of the fan c.g. to the point of attachment on the shaft. The fan offset distance increases the total fan transverse moment of inertia, which also leads to a reduction of the effective gyroscopic stiffening moment transmitted to the shaft. These two effects will combine to reduce the first critical speed as predicted by rigid, centered disc theory.

In order to simulate the influence of disc flexibility in the earlier critical speed analysis, the fan polar moment of inertia was derated. When the critical speed calculations were performed using only 10 % of the fan disc polar moment of inertia value I_p, the predicted first critical speed reduced from 3,577 RPM to 1,723 RPM. This value was in good agreement with the original experimental data observed on the B fan with the IRD equipment.

Table 1 shows that the fan is modeled as an offset disc with its center of gravity from the point of attachment at station 16 at a distance of 3.75 in. The rotational spring rate K_r attaching the disc to the shaft was assumed to be 1.35E7 in-lb/rad.

3.2.2 Influence of Fan End Bearing on Critical Speed.

One of the major influences on the rotor first critical speed is the combined effective stiffness of the fan end bearing and pedestal. A strain energy distribution for the 1*st* mode shows that 35-40 % strain energy may be associated with the fan end bearing, as compared to only 5 % for the motor end bearing. With a rigid disc, the reduction of bearing stiffness from 2.0E6 to 1.5E6 lb/in decreases the predicted critical speed from 3,577 RPM to 2,420 RPM, a reduction of 1,157 RPM.

The experimental data indicated that there was a considerable amount of pedestal motion. The pedestal influence was included in the critical speed model by representing it as a stiffness of K_f = 1.5E6 lb/in and an effective pedestal mass of 280 lb. The inclusion of pedestal effects causes a reduction of the overall effective bearing stiffness, and hence leads to a reduction in the predicted first critical speed.

3.2.3 Critical Speed Analysis of B Fan With 22 In. Bearing Span.

A model of the B fan with an offset fan wheel, and rolling element bearings mounted on flexible bearing pedestals is shown in Table 1. Figure 10 represents the animated first critical speed mode shape for the B fan with a 22 in. bearing span. This model shows a first critical speed of 1,662 RPM which corresponds well with the observed value on startup. The coastdown value may be observed at the lower speed due to the reduction in drive torque and nonlinear effects in the rolling element bearings.

Figure 10 shows that the maximum motion occurs at the fan location. A vibration pickup situated between the bearings might record little motion since this is close to a node point of the mode shape. The mode shape shows that the motion at the two bearings should be out of phase with twice the motion at the fan bearing as compared to the motor end bearing. The amplitude of motion of the mode shape as shown is dimensionless, and represents the

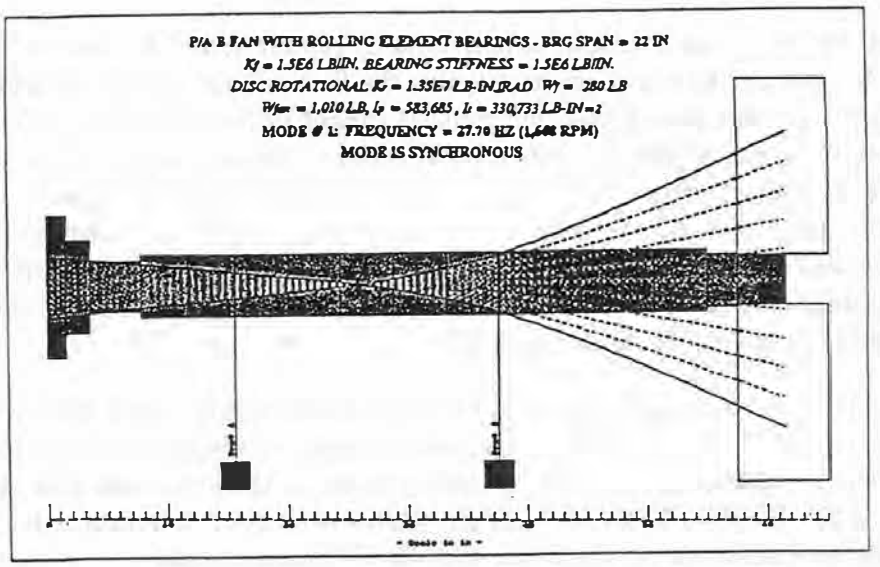

FIGURE 10. ANIMATED 1ST CRITICAL SPEED MODE SHAPE

TABLE 2. 1ST CRITICAL SPEED MODE SHAPE - 1,662 RPM

P/A B FAN WITH ROLLING ELEMENT BEARINGS-Wf=280 Lb,Kf=1.5E6 Lb/IN.
BEARING STIFFNESS = 1.5E6 Lb/In., DISC ROTATIONAL Kr=1.35E7 Lb-IN./rad
BEARING SPAN = 22 IN. , Wfan=1,010 Lb ,Ip=583,685, It=330,733 Lb-In^2

UNDAMPED ROTOR MODESHAPE & ENERGY DISTRIBUTION
SYNCHRONOUS CRITICAL SPEED ANALYSIS

FIRST CRITICAL SPEED = 1661.89 RPM (27.70 HZ) Delta = 6.50e-08

ST. #	X DIM	THETA SLOPE	M MOMENT	V SHEAR	Ushaft STRAIN ENERGY %	Ubrg ENERGY %	KeTran KINETIC ENERGY %	KeRot ENERGY %
1	-0.205	0.01	0.0	0.0			0.1	0.0
2	-0.193	0.01	-0.5	-0.4			0.2	0.0
3	-0.178	0.01	-2.3	-0.9			0.1	0.0
4	-0.146	0.01	-7.3	-1.2			0.0	0.0
5	-0.117	0.01	-12.6	-1.4			0.0	0.0
6	-0.088	0.01	-18.7	-1.6	0.2	4.5	0.0	0.0
7	-0.055	0.01	262.0	63.8	1.3		0.0	0.0
8	-0.016	0.01	542.3	63.7	3.6		0.0	0.0
9	0.035	0.01	822.4	63.7	7.0		0.0	0.0
10	0.102	0.02	1102.8	63.7	11.7		0.0	0.0
11	0.193	0.02	1384.1	63.9	11.0	21.7	0.1	0.0
12	0.310	0.03	1036.0	-79.6	5.7		0.3	0.0
13	0.449	0.03	690.4	-79.0	2.1		0.6	0.0
14	0.602	0.04	348.7	-78.1			1.1	0.0
15	0.762	0.04	11.9	-77.0			1.2	0.0
**	0.941	0.023			3.8		110.6	-16.8
16	0.854	0.04	-177.9	-75.9			1.1	0.0
17	1.000	0.04	0.0	-0.6			0.9	0.0
					42.91%	26.26%	5.83%	0.00%
Total Rotor Energy								
** Flexible Disk Energy					3.79%		110.56%	-16.78%

Brg #	St. #	K Brg Lb/In	K Eff Lb/In	Xbrg DIM	Xsup DIM	Ubrg %	Usup %	KE Sup %
1	6	1500000	744467	-0.09	-0.04	4.51	4.65	0.07
2	11	1500000	744467	0.19	0.10	21.75	22.40	0.33

U Total = 3.17e+04 KE Total = 3.17e+04 Energy Balance = 0.00 % Error

to the shaft. When the fan polar moment of inertia I_p is greater than the fan transverse moment of inertia I_t , the gyroscopic moment elevates the first critical speed. If, however, the fan disc flexes, then the complete gyroscopic moment cannot be transmitted to the shaft. This causes a reduction in the predicted rotor critical speed. Another factor which causes a reduction in the gyroscopic moment transferred is the fan axial offset distance of the fan c.g. to the point of attachment on the shaft. The fan offset distance increases the total fan transverse moment of inertia, which also leads to a reduction of the effective gyroscopic stiffening moment transmitted to the shaft. These two effects will combine to reduce the first critical speed as predicted by rigid, centered disc theory.

In order to simulate the influence of disc flexibility in the earlier critical speed analysis, the fan polar moment of inertia was derated. When the critical speed calculations were performed using only 10 % of the fan disc polar moment of inertia value I_p, the predicted first critical speed reduced from 3,577 RPM to 1,723 RPM. This value was in good agreement with the original experimental data observed on the B fan with the IRD equipment.

Table 1 shows that the fan is modeled as an offset disc with its center of gravity from the point of attachment at station 16 at a distance of 3.75 in. The rotational spring rate K_r attaching the disc to the shaft was assumed to be 1.35E7 in-lb/rad.

3.2.2 Influence of Fan End Bearing on Critical Speed.

One of the major influences on the rotor first critical speed is the combined effective stiffness of the fan end bearing and pedestal. A strain energy distribution for the $1st$ mode shows that 35-40 % strain energy may be associated with the fan end bearing, as compared to only 5 % for the motor end bearing. With a rigid disc, the reduction of bearing stiffness from 2.0E6 to 1.5E6 lb/in decreases the predicted critical speed from 3,577 RPM to 2,420 RPM, a reduction of 1,157 RPM.

The experimental data indicated that there was a considerable amount of pedestal motion. The pedestal influence was included in the critical speed model by representing it as a stiffness of K_f = 1.5E6 lb/in and an effective pedestal mass of 280 lb. The inclusion of pedestal effects causes a reduction of the overall effective bearing stiffness, and hence leads to a reduction in the predicted first critical speed.

3.2.3 Critical Speed Analysis of B Fan With 22 In. Bearing Span.

A model of the B fan with an offset fan wheel, and rolling element bearings mounted on flexible bearing pedestals is shown in Table 1. Figure 10 represents the animated first critical speed mode shape for the B fan with a 22 in. bearing span. This model shows a first critical speed of 1,662 RPM which corresponds well with the observed value on startup. The coastdown value may be observed at the lower speed due to the reduction in drive torque and nonlinear effects in the rolling element bearings.

Figure 10 shows that the maximum motion occurs at the fan location. A vibration pickup situated between the bearings might record little motion since this is close to a node point of the mode shape. The mode shape shows that the motion at the two bearings should be out of phase with twice the motion at the fan bearing as compared to the motor end bearing. The amplitude of motion of the mode shape as shown is dimensionless, and represents the

Figure 10 shows that the maximum motion occurs at the fan location. A vibration pickup situated between the bearings might record little motion since this is close to a node point of the mode shape. The mode shape shows that the motion at the two bearings should be out of phase with twice the motion at the fan bearing as compared to the motor end bearing. The amplitude of motion of the mode shape as shown is dimensionless and represents the relative vibration of the shaft at the critical speed. The maximum motion is normalized to unity. (*Actual rotor motion must be computed with a forced response program which includes rotor unbalance and bearing damping*). The dimensionless mode shape for the first mode is shown in Table 2.

Table 2 shows, for example, that the amplitude at the overhung fan location should be 5 times the motion observed at the fan bearing. If the air seal is assumed to be located at station 15, then the motion at this location will be over 4 times the motion obtained at the fan bearing. Thus, high fan end bearing motion will imply large amplitudes of motion at the air seal location with subsequent wear of this component. (For example, 5 mils of absolute motion at the fan bearing will indicate over 20 mils of motion at the air seal). Therefore, it will be difficult to maintain close seal clearances with the current configuration.

Table 2 represents the mode shape and energy distribution for the first mode. At the bottom of Table 2 is a summary of the bearing and support motions and energy distributions. The combined bearing/support strain energy for the fan bearing (Brg. # 2 at st. 11) is 44 %. This indicates that the fan bearing has a major influence on the value of the first critical speed. Note that Table 2 shows a combined effective bearing impedance or stiffness of K_{eff} = 744,467 lb/in. This reduction in stiffness below the bearing stiffness of K_{brg} = 1.5E6 lb/in is caused by the influence of the pedestal mass and flexibility.

3.3 Critical Speed Summary.

A model was developed for the overhung fans and the critical speeds were calculated including various effects of bearing stiffness, bearing span, and fan disc characteristics. The B fan is operating at a speed slightly higher than its critical speed. Figure 11 represents a critical speed map of the P/A fan with the standard bearing span and with rigid and flexible offset discs. From the critical speed map, it is seen that with nominal bearing stiffness values of 1.0E6 lb/in., the fan is operating slightly above the critical speed. When the B fan passes through the critical speed, the bearing forces are greatly reduced. The A, C, and D fans are operating in the subcritical speed region under conditions of high bearing loading and reduced life conditions. As these bearings wear, the effective bearing stiffness reduces, causing the critical speed to drop closer to the operating speed. This means that, with time, the bearing amplification factors continue to increase causing a progressive deterioration of the bearings.

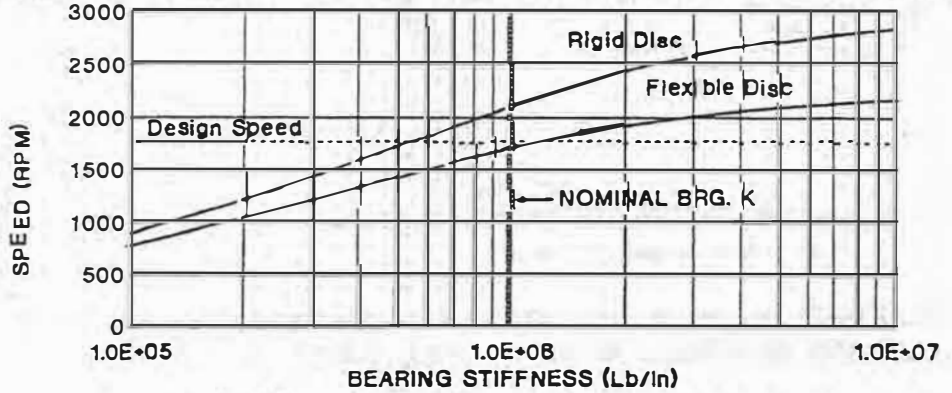

FIGURE 11. CRITICAL SPEED MAP OF P/A FAN

4 FAN UNBALANCE RESPONSE

4.1 Unbalance Response of B Fan With Rolling Element Bearings.

A reduced 8 station model was generated to simulate the 17 station model with similar critical speed and modal properties. A number of forced response calculations were performed on the rotor with various conditions of unbalance in order to determine the actual amplitudes of motion and to determine the bearing forces transmitted (*Salamone and Gunter, 78*). Figure 12 represents the amplitude and phase of the fan, seal, and bearings for the B fan for 100 gm-in. of radial unbalance with rolling element bearings. The unbalance of 100 gm in. causes a maximum response of 20 mils (*peak to peak*) at the fan location. The motion at the fan end bearing is approximately 3.3 mils (*peak to peak*). Therefore, the fan motion is over 6 times greater than the motion recorded at the fan end bearing.

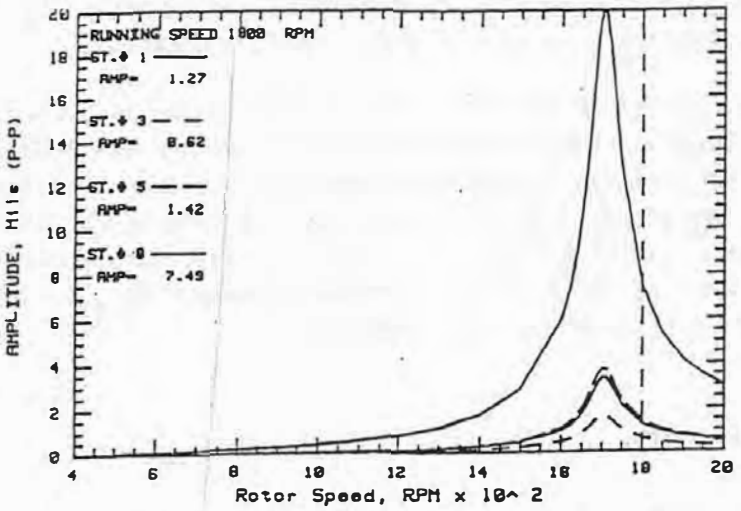

FIGURE 12. FAN AND MOTOR END BEARING AMPLITUDE WITH ROLLING ELEMENT BEARINGS

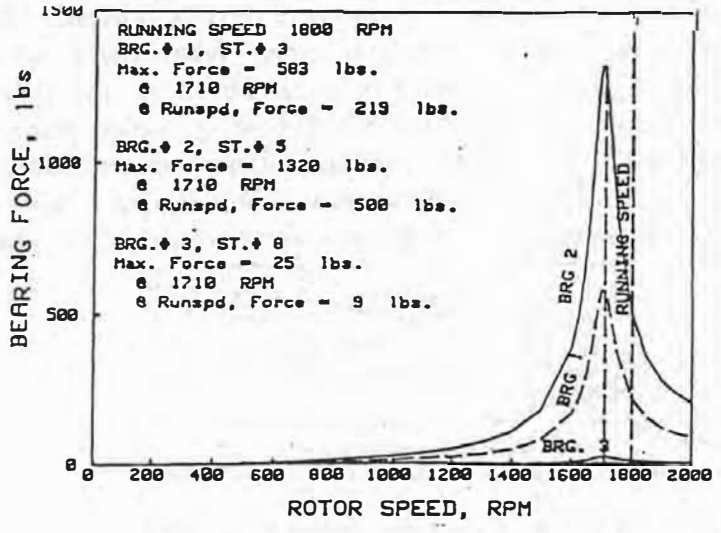

FIGURE 13. BEARING FORCES TRANSMITTED VS. SPEED WITH ROLLING ELEMENT BEARINGS - 100 GM-IN. UNBALANCE

Figure 13 represents the bearing forces transmitted at the motor bearing (station 3), fan bearing (station 5), and fan air seal (station 8). Figure 13 shows that, at the critical speed of 1,710 RPM, the transmitted fan bearing force is 1,320 lb which is generated by a rotating load of only 18 lb. This represents a dynamic transmissibility ratio TRD of over 72. At the operating speed of 1,800 RPM, the rotating unbalance is 20 lb at design speed and the transmitted fan bearing force reduces to 500 lb. This represents a dynamic transmissibility of 25. This value is excessive if long bearing life is to be obtained. Note that a reduction of overhang to increase the critical speed will also result in large bearing forces transmitted to the fan end bearing due to subcritical speed operation.

4.2 Unbalance Response of A Fan with Fluid Film Bearings.

The unbalance response of the A fan in fluid film bearings with 100 gm-in. was simulated as shown in Figure 14. It can be seen that the fan is operating on top of the critical speed. Although the A fan is operating in the critical speed region, the fan bearing transmitted force is only 162 lb as compared to 500 lb for the rolling element bearing configuration as shown in Figure 15. This value represents a TRD of 8. Thus, changing from rolling element to fluid film bearings will reduce the bearing loads by a factor of 3.

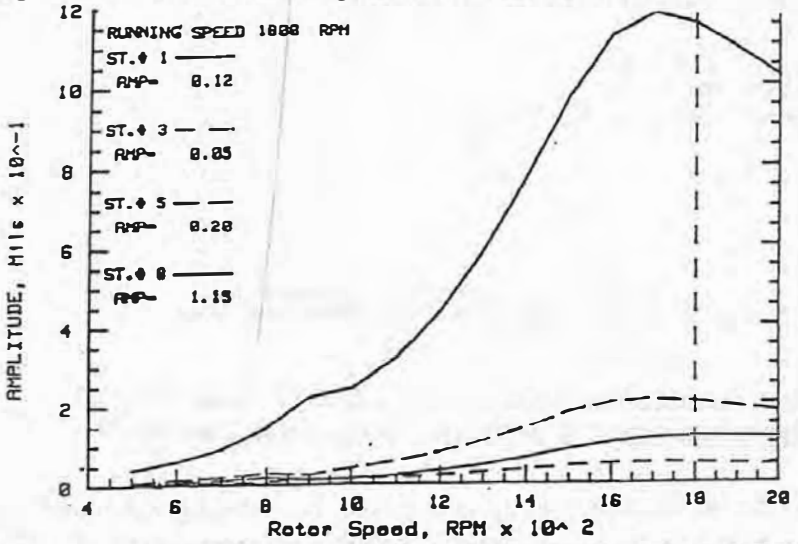

FIGURE 14. OVERHUNG P/A FAN IN FLUID FILM BEARINGS 100 GM-IN. UNBALANCE, BEARING SPAN = 22 IN.

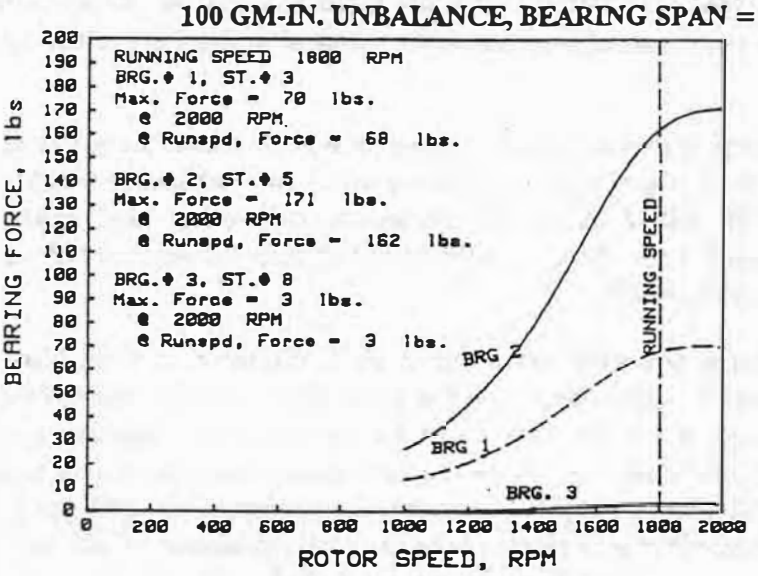

FIGURE 15. BEARING FORCES TRANSMITTED VS. SPEED WITH FLUID FILM BEARINGS - 100 GM-IN UNBALANCE

A simulation was performed in which the overhung shaft diameter was reduced in order to reduce the fan critical speed.

Figure 16 represents the bearing forces transmitted with fluid film bearings and a reduced shaft diameter from 4.0 to 3.5 in. at the overhang location. By reducing the shaft diameter, the fan 1*st* critical speed is reduced to 1,340 RPM. The maximum force transmitted at the critical speed is 204 lb. At running speed, the fan end bearing force reduces to 88 lb. This represents a dynamic transmissibility of 4. Hence, it is seen that reducing the shaft overhang diameter will result in a bearing force reduction of 1/2 from the case of the original shaft design in fluid film bearings. The use of a reduced shaft diameter and fluid film bearings represents a 6 fold reduction in forces in comparison to the B fan mounted in rolling element bearings.

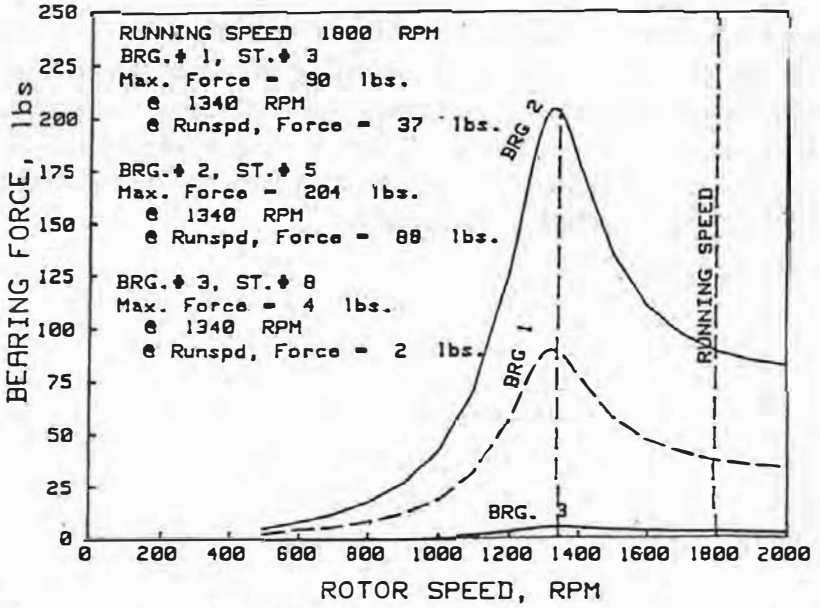

FIGURE 16. BEARING FORCES VS. SPEED WITH FLUID FILM BEARINGS AND REDUCED SHAFT OVERHANG DIAMETER -100 GM-IN

It is seen that the bearing forces may be greatly attenuated by reducing the shaft diameter at the overhang and using fluid film bearings instead of rolling element bearings. The speed range of the shaft is such that oil whirl stability problems will not be encountered. This design change, however, is not practical because of the physical limitations of the fan and air seal design.

The excitation of the overhung fan wheel may be caused by a single plane fan radial unbalance, or by a couple unbalance. A couple unbalance is generated by two unbalance weights of equal magnitude but situated 180° out of phase with respect to each other and separated by a distance *t*. With an overhung rotor, it is difficult to distinguish between radial and couple unbalance (*Salamone and Gunter, 80*).

The response of the overhung fan with the reduced shaft diameter in fluid film bearings excited by couple unbalance of 1,000 gm-in. with a plane separation of approximately 8 in was computed. The response of the fan appears to be similar to the response caused only by a single radial plane of unbalance. By comparing the values of bearing forces transmitted at running speed, it is seen that a couple unbalance of approximately 200 gm-in. (1,600 gm-in^2)will produce the same effect as a single plane of radial unbalance of 100 gm-in. If the fan shaft should become warped, this will produce a skew of the disk, which will produce a rotor response similar to fan couple unbalance.

In the balancing process, if one should encounter high vibration at the motor end bearing, after single plane radial balancing of the fan, then couple balancing of the fan should be considered.

4.3 Unbalance Response of B Fan With Rolling Element Bearings and Isolation Pad With Fan End Bearing

The dynamic characteristics of the standard B fan mounted in rolling element bearings were analyzed with isolation pads mounted under one or more of the fan bearing pedestals. From the critical speed analysis, it is seen that approximately half the system strain energy is associated with the fan end bearing and support. Hence, a reduction of the fan end effective bearing stiffness will lower the critical speed below the operating speed range of the fan.

Figure 17 represents the fan amplitude of motion with 100 gm-in. of unbalance and a rubber isolation pad of stiffness 300,000 lb/in. and damping of 5 lb-sec/in. This isolation pad reduces the fan 1st critical speed to 1,150 RPM. It is of interest to note that if a second isolation pad is placed at the motor end bearing, then one may encounter a second critical speed at the operating speed. The fan motion at running speed with the isolation pad is only 0.70 mils (*peak to peak*) and only 0.24 mils (*peak to peak*) at the fan end bearing. Thus the fan with this design concept is very insensitive to unbalance.

Figure 18 represents the bearing force transmitted with an isolation pad mounted under the fan end bearing pedestal. At the critical speed of 1,150 RPM, the fan end bearing force is 409 lb. This value reduces to only 39 lb at running speed. Since the rotating load is slightly less than 20 lb due to the 100 gm-in unbalance, this bearing force magnitude is approaching the theoretical static bearing load of twice the fan loading. This represents the lowest bearing loading possible in which the fan overhang distance is equal to the bearing span.

From this analysis, it is seen that the bearing forces transmitted with the rolling element bearings may be reduced by a factor of **25** with a properly designed isolation support.

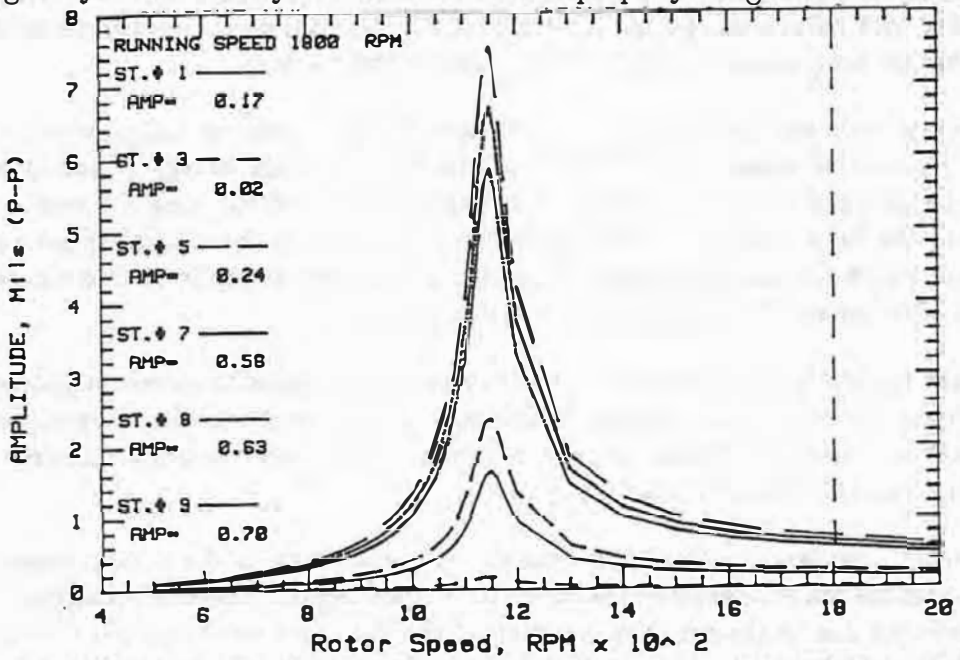

FIGURE 17. OVERHUNG FAN AMPLITUDE OF MOTION WITH ROLLING ELEMENT BEARINGS WITH FAN END BEARING PEDESTAL ISOLATION PAD - K_f = 300,000 LB/IN. ,C_f = 5 LB-SEC/IN.

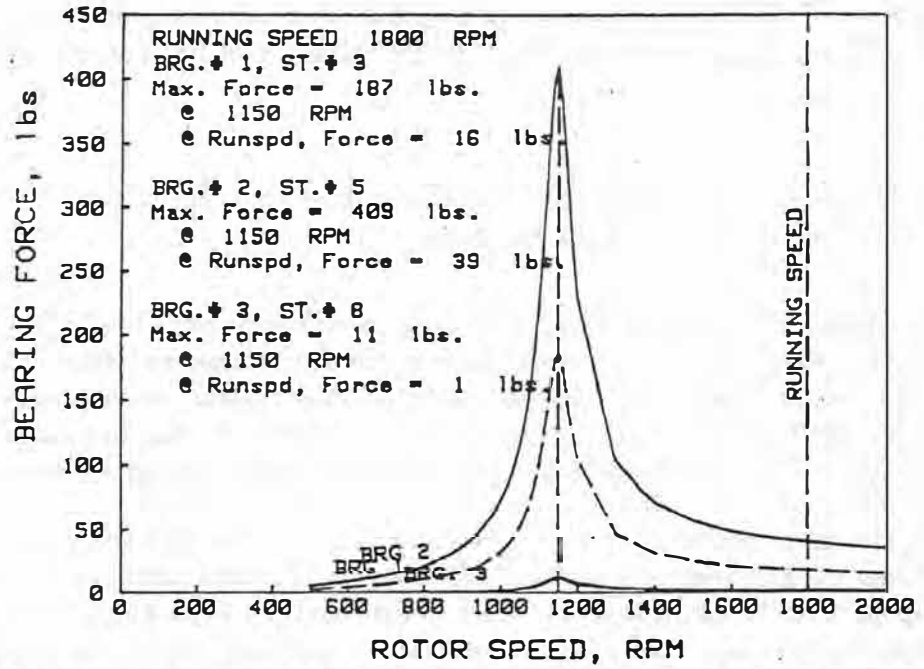

FIGURE 18. BEARING FORCES VS SPEED WITH ROLLING ELEMENT FAN BEARING PEDESTAL ON ISOLATION PAD - K_r = 300,000 LB/IN.

5 Discussion and Conclusions

The overhung P/A fans were designed to operate as subcritical speed rotors. However, it was found that the fans do not operate 20 % below the 1*st* critical speed as originally designed. Attempts to simulate the fan behavior showed that the B fan rotor on rolling element bearings with the standard bearing span is operating slightly above the 1*st* critical speed.

Accurate critical speed calculations could not be made based on rigid disk theory with this class of fan wheel. The fan wheels are flexible and this reduces the amount of gyroscopic moment that may be transmitted to the shaft, the flexible fan effect may be treated by an offset disc attached to a rotational spring. An equivalent rotational disc attachment spring rate may be estimated using experimental or finite element techniques.

The fan end pedestal mass and flexibility is an important factor as well as disk flexibility in determining the fan critical speed. Almost 50 % of the system strain energy is associated with the fan end bearing and support. Increasing the bearing span and reducing the overhang distance to elevate the 1*st* critical speed did not sufficiently increase the critical speed to a significant distance above the operating speed. Subcritical speed operation in rolling element bearings leads to high values of transmitted fan bearing forces.

The rolling element fan end bearings degrade rapidly causing high superharmonic vibrations. Nonlinear dead band behavior is experienced in the fans after several months of operation. Thus, the current fan design in rolling element bearings cannot hold balance due to the extreme sensitivity coupled with coal dust build-up.

The effective bearing impedance in fluid film bearings is higher than in the rolling element bearings. This causes the fan to operate in the subcritical speed region. However, transmitted bearing forces are lower due to the superior damping of the fluid film bearings. No evidence of self-excited oil film whirl was observed with the use of the fluid film bearings. The fan in fluid film bearings may be adequately balanced by using both motor and fan end vibration data.

REFERENCES

1. Barrett, L. E., Gunter, E. J., and Allaire, P. E., *Optimum Bearing and Support Damping for Unbalance Response and Stability of Rotating Machinery*, **Engineering for Power, ASME Trans.**, December 1976.

2. Benson, R. C. *Dynamic Response of an Overhung Unbalanced Skewed Rotor in Fluid Film Bearings*, **M.S. Thesis, University of Virginia**, August 17, 1974.

3. Colen, R. B., and Gunter, E. J., *Undamped Critical Speed Analysis of Rotor Systems - A Manual for Use With Computer Program CRTSPD*, **Report No. UVA/643078/MAE81/105**, June 1981.

4. Gaston, C. G. and Gunter, E. J., **CRITSPD-PC - User's Manual for Undamped Critical Speed Analysis of Flexible Rotor-Bearing Systems**, RODYN Vibration, Inc., Charlottesville, Virginia, August 1987.

5. Kazao, Y. and Gunter, E. J., *Dynamics of Multi-Spool Gas Turbines Using the Transfer Matrix Method - Theory and Applications*, **Proceedings of International Conference on Mechanical Dynamics**, August 3-6, 1987, Shenyang, China, Press of Northeast University of Technology, pp. 24-29.

6. Kikuchi, K., *Analysis of Unbalance Vibration of Rotating Shaft System With Many Bearings and Disks*, **JSME Bulletin**, June 16, 1969.

7. Kirk, R. G. and Gunter, E. J., *The Effects of Support Flexibility and Damping on the Synchronous Response of a Single Mass Flexible Rotor*, **Journal of Engineering for Industry, ASME Trans.**, 94.1 Series B, pp. 221-232, February 1972.

8. Lund, J. W. and Shomsen, K. K., *A Calculation Method and Data for the Dynamic Coefficients of Oil-Lubricated Journal Bearings*, **Topics in Fluid Film Bearings and Rotor Bearing System Design and Optimization, ASME**, 1978, pp. 1-28.

9. Peterson, Ken, Editor, **MSC/PAL2 User's Manual**, The MacNeal-Schwendler Corporation, 815 Colorado Boulevard, Los Angeles, California, November 1987.

10. Prohl, M. A., *A General Method for Calculating Critical Speeds of Flexible Rotors*, **Journal of Applied Mechanics, Trans. ASME**, Vol. 67, 1945.

11. Salamone, D. J. and Gunter, E. J., *Effects of Shaft Warp and Disk Skew on the Synchronous Unbalance Response of a Multi Mass Rotor in Fluid Film Bearings*, **Topics in Fluid Film Bearings and Rotor Bearing System Design and Optimization, ASME**, 1978, pp. 79-107.

12. Salamone, D. J., and Gunter, E. J., *Synchronous Unbalance Response of an Overhung Rotor with Disk Skew*, **ASME Journal of Engineering for Power**, Vol. 102 (October 1980), pp. 749-755.

APPENDIX
Equations of Motion of a Cantilevered Impeller Disc

1 Kinetic Energy

A disc is cantilevered from a rotor mass station i by a distance h (see Fig. 1). At the point of attachment to the shaft at point c, the cantilevered section is connected by a rotational spring of K_r in-lb. The torsional or rotational flexibility is due to the elasticity of the cone element.

The kinetic energy of the disc is given by:

$$T = T_{trans} + T_{rotational} \tag{1.1}$$

Where:

$$T_{trans} = \frac{1}{2} m_d (\dot{X}_d^2 + \dot{Y}_d^2)$$

$$T_{rotational} = \frac{1}{2} I_t (\dot{\Theta}_{xd}^2 + \dot{\Theta}_{yd}^2) + \frac{1}{2} I_p [\omega^2 + \omega(\dot{\Theta}_{xd}\Theta_{yd} - \dot{\Theta}_{yd}\Theta_{xd})]$$

$$\left.\begin{array}{l} X_d = X + h\Theta_{xd} \\ Y_d = Y + h\Theta_{yd} \end{array}\right\} \text{ for small angles} \tag{1.2}$$

The translational kinetic energy is given by:

$$T_{trans} = \frac{1}{2} m_d[(\dot{X} + h\dot{\Theta}_{xd})^2 + (\dot{Y} + h\dot{\Theta}_{yd})^2] \tag{1.3}$$

2 Lagrange's Equations of Motion

Lagrange's Equations of motion are given by

$$\frac{d}{dt}\left(\frac{\partial T}{\partial \dot{q}_r}\right) - \frac{\partial T}{\partial q_r} + \frac{\partial V}{\partial q_r} + \frac{\partial \mathcal{D}}{\partial \dot{q}_r} = F_{qr} \tag{2.1}$$

2.1 Lateral Equations of Motion - X, Y

The equation of motion for the X direction is given by

$$\frac{d}{dt}\left(\frac{\partial T}{\partial \dot{X}}\right) - \frac{\partial T}{\partial X} = m_d (\ddot{X} + h\ddot{\Theta}_{xd}); F_x = \text{Generalized X component of force} \tag{2.2}$$

$$m_d (\ddot{X} + h\ddot{\Theta}_x d) = F_x = \sum \vec{F}_{ex} \cdot \frac{\partial \vec{V}}{\partial \dot{X}} \tag{2.3}$$

If shaft mass and station shear effects are included in the equations, then the complete equation of motion for the i^{th} station is given by:

$$m_s \ddot{X} + m_d (\ddot{X} + h\ddot{\Theta}_{xd}) = V_r^{(i-1)} - V_r^{(i)} - K_i X$$

$$V_r^{(i)} = V_r^{(i-1)} - K_i X - m_s \ddot{X} - m_d (\ddot{X} + h\ddot{\Theta}_{xd}) \tag{2.4}$$

For a rigid disc, $\Theta_{xd} = \Theta_{xs}$; $\Theta_{yd} = \Theta_{ys}$
For synchronous precession, $\ddot{X} = -\nu^2 X$ and $\ddot{\Theta}_s = -\nu^2 \Theta_s$

Hence the shear equation for a rigidly offset disc is given by

$$V_r^{(i)} = V_r^{(i-1)} + ((m_s + m_d)\nu^2 - K_i)X + m_d \nu^2 h\Theta_s$$

$$\begin{aligned} Let\ \bar{V}_r &= V_r\, L_{3avg}\ ;\ L_{3avg}\ is\ a\ scaling\ factor \\ \bar{\Theta}_s &= \Theta_s\, L_{avg} \end{aligned}$$

$$\bar{V}_r^{(i)} = \bar{V}_r^{(i-1)} + ((m_s + m_d)\nu^2 - K_i) L_{3avg} X + m_d\, \nu^2 h \frac{L_{3avg}}{L_{avg}} \bar{\Theta}_s \tag{2.5}$$

For a flexible disk (see Eq. 2.12 for a complete derivation of I)

$$\bar{\Theta}_{dx} = \bar{I}\bar{\Theta}_{sx} + \nu^2 \frac{m_d h}{K_r} \bar{I} L_{avg} X$$

The shear equation with a flexible disc is:

$$\bar{V}_r^{(i)} = \bar{V}_r^{(i-1)} + [((m_s + m_d)\nu^2 - K_i) L_{3avg} + (m_d\, \nu^2\, h)^2 \frac{\bar{I}}{K_r} L_{3avg}] X + m_d \nu^2 h \frac{L_{3avg}}{L_{avg}} \times \bar{I}\bar{\Theta}_{sx}$$

2.2 Offset Disc Rotational Equations of Motion - Θ_{xd}, Θ_{yd}

The strain energy for the bearing stiffness at the i^{th} station and the torsional restoring moment connecting the cantilevered disk to the i^{th} station may be expressed as:

$$V = \frac{1}{2}[K_x X_i^2 + K_y Y_i^2] + \frac{1}{2} K_r [(\Theta_{xd} - \Theta_{xs})^2] + \frac{1}{2} K_r [\Theta_{yd} - \Theta_{ys}]^2 \tag{2.6}$$

In general, circular orbits will be assumed.
The equation of motion corresponding to the disk rotation angle Θ_d is given by:

$$\frac{d}{dt}\left(\frac{\partial T}{\partial \dot{\Theta}_{xd}}\right) - \frac{\partial T}{\partial \Theta_{xd}} + \frac{\partial V}{\partial \Theta_{xd}} = F_{\Theta xd} \tag{2.7}$$

The generalized moment $F_{\Theta xd}$ is given by

$$F_{\Theta xd} = \vec{M}_{\Theta xd} \cdot \frac{\partial \vec{\omega}}{\partial \dot{\Theta}_{xd}}$$

Where

$\vec{M}_{\Theta xd}$ = Vector moments acting on disc in X-Z slope

The rotational equation of motion corresponding to the disc angle Θ_{xd} is given by

$$m_d h \ddot{X} + (m_d h^2 + I_t)\, \ddot{\Theta}_{xd} + \omega I_p\, \dot{\Theta}_{yd} + K_r\, (\Theta_{xd} - \Theta_{xs}) = 0 \tag{2.8}$$

Assuming circular forward precession

$$X(t) = X e^{i\nu t}\ ;\ \ddot{X} = -\nu^2 X$$

Assume that the disc and shaft centerline moves in a forward circular orbit as given by

$$\begin{aligned} \Theta_{xd} &= \Theta_d \cos \nu t \quad \Theta_{xs} = \Theta_s \cos \nu t \\ \Theta_{yd} &= \Theta_d \sin \nu t \quad \Theta_{ys} = \Theta_s \sin \nu t \end{aligned}$$

where Θ_d = cone angle of motion of disc
Θ_s = cone angle of motion of shaft centerline at station i
$\ddot{\Theta}_{xd} = -\nu^2\, \Theta_d \cos \nu t = -\nu^2 \Theta_{xd}$
$\dot{\Theta}_{yd} = \nu\, \Theta_d \cos \nu t = \nu \Theta_{xd}$

Therefore Eq. 2.8 for circular synchronous precession reduces to

$$-\nu^2 m_d h X + \nu\left[\omega I_p - \nu(m_d h^2 + I_t)\right]\Theta_d + K_r\Theta_d = K_r\Theta_s \tag{2.9}$$

$$\text{Let } I = \omega\nu I_p - \nu^2(m_d h^2 + I_t)$$

Then equation 2.9 can be written as:

$$(I + K_r)\Theta_d = K_r\Theta_{xs} + \nu^2 m_d h X \tag{2.10}$$

solving for Θ_d

$$\Theta_d = \frac{K_r\Theta_{xs}}{I + K_r} + \frac{\nu^2 m_d h}{I + K_r} X \tag{2.11}$$

$$\text{Let}\bar{I} = \frac{K_r}{I + K_r} = \frac{1}{1 + I\,K_r}$$

$$\bar{\Theta}_d = L_{avg}\Theta_d$$

$$\bar{\Theta}_d = \bar{I}\bar{\Theta}_{xs} + \nu^2 m_d h\frac{\bar{I}}{K_r}L_{avg}X \tag{2.12}$$

2.3 Shaft Rotational Equation of Motion Θ_s

The equation of motion for the shaft angular motion Θ_s is similar to the equation of motion Θ_d for the disc. The values of I_{ps} and I_{ts} are the disc mass moment of inertia effects acting directly at the i^{th} mass station

$$\frac{d}{dt}\left(\frac{\partial T}{\partial\dot{\Theta}_s}\right) - \frac{\partial T}{\partial\Theta_s} + \frac{\partial V}{\partial\Theta_s} = F_{\Theta s} = M_L^{(i)} - M_R^{(i-1)} \tag{2.13}$$

The disc equation of motion in the fixed X-Z plane at the shaft station i is given by

$$I_{ts}\ddot{\Theta}_{xs} + \omega\, I_{ps}\,\dot{\Theta}_{ys} + K_r(\Theta_{sx} - \Theta_{dx}) = M_L^{(i)} - M_R^{(i-1)} \tag{2.14}$$

Assuming circular synchronous precession, $\Theta_s = \Theta_{sx} + i\Theta_{sy}$

$$M_L^{(i)} = M_R^{(i-1)} + \nu(\omega I_{ps} - \nu I_{ts})\Theta_s + K_r(\Theta_s - \Theta_d) \tag{2.15}$$

The disc motion Θ_d may be eliminated from Eq. 2.15 by Eq. 2.11

$$K_r(\Theta_s - \Theta_d) = I\bar{I}\Theta_s - \nu^2 m_d h\bar{I}X$$

The moment equation (2.15) is thus given by

$$M_L^{(i)} = M_R^{(i-1)} + \left[\nu\,(\omega I_p s - \nu\, I_{ts}) + I\bar{I}\right]\Theta_s - \nu^2\, m_d h\bar{I}\, X \tag{2.16}$$

Since M and Θ are expressed in a normalized form as follows

$$\bar{M} = M L_{2avg} \quad , \quad \Theta = \Theta L_{avg}$$

Eq. 2.16 in normalized form is written as

$$\bar{M}_L^{(i)} = \bar{M}_{R(i-1)} + \left[\nu\,(\omega I_{ps} - \nu\, I_{ts}) + I\,\bar{I}\right]\frac{L_{2avg}}{L_{avg}}\Theta_s - \nu^2\, m_d h\,\bar{I}\,L_{2avg}\,X \tag{2.17}$$